Article

JOURNAL OF COMPOSITE MATERIALS

Journal of Composite Materials
0(0) 1–15

DOI: 10.1177/00219983211032390
journals.sagepub.com/home/jcm
SAGE

Fresh and hardened state performance of self-compacting slag based alkali activated concrete using nanosilica and steel fiber

Necip Altay Eren[1], Radhwan Alzeebaree[2,3], Abdulkadir Çevik[1], Anıl Niş[4], Alaa Mohammedameen[2,3] and Mehmet Eren Gülşan[1]

Abstract

This study investigates the fresh and hardened state performance of slag-based self-compacting alkali-activated concretes (SCAAC) reinforced with steel fibers (SF) and nano-silica (NS), cured at an ambient temperature. Two different hooked-end SF with two fiber volumes and NS were used to examine the combined effect of the SF volume ratio, SF aspect ratio, and NS on the fresh and hardened state performance of SCAAC. In extension, the influence of specimen thickness to steel fiber length (d/F_L) ratio on the failure modes of the bending specimens was evaluated. The fresh state properties were evaluated via T_{50} value, slump flow, V-funnel, and L-Box tests, while the hardened state properties were studied through compressive strength, splitting tensile strength, modulus of elasticity, and flexural tensile strength tests. The relationship analyses were carried out among fresh and hardened state properties, and scanning electron microscopy (SEM) was also conducted to examine the microstructure. The results indicated that fresh state performance was favorably affected by NS inclusion but adversely influenced by SF content and aspect ratio. The hardened state performances enhanced with a higher amount of SF volume and an aspect ratio. Also, the NS improved the splitting tensile and flexural strength but decreased the compressive strength and elasticity modulus of the specimens. The d/F_L ratio was found a significant parameter on failure modes, and the specimens having a d/F_L ratio of 3.33 showed flexural cracks. In contrast, the specimens having a d/F_L ratio of 1.25 exhibited inclined flexural-shear cracks, especially for 1% SF.

Keywords

Self-compacting alkali activated concrete, nano-silica, steel fiber, modulus of elasticity, tensile strength and fresh state properties

Introduction

One of the most significant environmental concerns is the climate crisis, which has been neglected for decades. Professor Raymond stresses the vital circumstance: "Let's get this on the table right away, without mincing words. With regard to the climate crisis, yes, it's time to panic. We are in deep trouble."[1] The development of environment-friendly and sustainable concrete is the current research interest to decrease the environmental degradation of ordinary Portland cement (OPC) concrete. For 1-ton OPC production, a large quantity of energy is required approximately 120–130 electricity units. It emits 0.6–0.75 ton CO_2 in the atmosphere, responsible for the greenhouse effect and 7% pollutants in atmosphere.[2] It is estimated that the world economy uses more than 1,00,000 million tons of natural resources (an average of 13 tons per person)

[1]Civil Engineering, Gaziantep University, Turkey
[2]Akre Technical Institute, Duhok Polytechnic University, Iraq
[3]Department of Architecture, Nawroz University, Iraq
[4]Department of Civil Engineering, Istanbul Gelisim University, Turkey

Corresponding author:
Anıl Niş, Department of Civil Engineering, Istanbul Gelisim University, Istanbul, Turkey.
Email: anis@gelisim.edu.tr

and only 8,400 million tons are recycled. Therefore, recycling can be a solution to concrete productions.

Some industrial wastes can be recycled through concrete technology applications such as ground granulated blast furnace slag, silica fume, and fly ash. For several decades, many researchers have practically used industrial mineral waste as an alternative to the cement. The cement production process releases a substantial amount of greenhouse gases into the atmosphere due to the decarbonization of limestone and the combustion of fossil fuels. Moreover, OPC is considered as the most energy-requiring material after steel and aluminum.[3,4] The substantial issues for both the future of mankind and the cement industry are the high amount of required energy and the undesirable effects of CO_2 on the atmosphere. Therefore, new friendly environment materials should be used as an alternative to OPC to solve environmental concerns.[5,6] Recently, an environment-friendly concrete, geopolymer concrete, has emerged as an alternative material instead of OPC concrete.[7,8] Geopolymer concrete (GPC) takes a significant interest due to the considerable reduction in both the requirement of natural resources and the amount of carbon dioxide emissions. Moreover, geopolymer concrete utilizes to produce advanced construction materials using a by-product alumina-silicate composition.[9,10] However, geopolymer concretes can show some shortcomings, including cost, carbon dioxide emissions, efflorescence, alkali-silica reaction, and steel rebar corrosion, depending on the binder, alkali activator, aggregate types and curing conditions.[11]

Self-compacting concrete (SCC) is a new type of concrete that its weight can consolidate without needing any external or internal mechanical vibration to fill the formwork.[12] In extension, the resistance to bleeding and segregation without loss of stability is one of the most significant interest in the utilization of SCC. The researchers have investigated the fresh and hardened state performance of SCC since the 1990s, when used in the construction industry.[13–15] It has been revealed that the binder content of 500–600 kg/m^3 is required to realize the SCC requirements by related guidelines/standards.[16] Furthermore, approximately one ton of CO_2 is produced during the production of one ton of cement; hence the extreme utilization of cement becomes uneconomical and undesirable. Therefore, researchers aimed to take advantage of mineral fillers or by-product cementitious materials like silica fume, ground granulated blast furnace slag (GGBFS), and fly ash. These materials are utilized to eliminate the expenditures and improve the workability, flowability, and mechanical performance of the matrix.[17–20] It was reported from earlier investigations that GGBFS, fly ash, and silica fume make favorable contributions to the concrete's mechanical and/or fresh state properties as economical and eco-friendly materials.[21,22]

The poor tensile strength and ductility of SCC led to the use of steel fibers to avoid this drawback.[23] The additions of steel fiber (SF) can improve the post-cracking, ductility, and toughness of the concrete.[21,24] In addition, steel fibrous self-compacted concretes achieve more acceptable cost to benefit ratios than non-fibrous self-compacted concrete.[25] The steel fiber content and steel fiber aspect ratio are considered the main factors for the design procedure and optimization technique to produce the SCC mixes.[26–28] Researchers have revealed that an optimal amount of SF is 1% for most structures due to economic considerations.[29]

The inclusion of SF improves the compressive strength, and this enhancement depends on the steel fiber content and aspect ratio.[30] The improvement of compressive strength due to the presence of the SF may become 20% compared to the compressive strength of specimens without SF.[31,32] However, the incorporation of steel fiber can improve the splitting tensile strength much more than the compressive strength, and the improvement in the tensile strength can reach up to 98% depending on the amount of SF.[32] The addition of SF also improves the drying shrinkage by bridging the micro-cracks created by the restrained shrinkage.[33,34] Furthermore, the addition of SF provides significant improvement regarding the flexural strength, propagation of cracks, post-failure ductility, and toughness.[24] In addition, the steel fiber increases the energy absorption and compressive ductility at an early age.[35]

Recently, researchers have investigated the utilization of nano-silica (NS) in the concrete industry.[36–40] The concrete quality, mainly depends on the properties of the interfacial transition zone (ITZ) between aggregate and hardened cement paste. The obtained findings indicated that the use of NS enhanced the microstructure and the finer hydrated phases (C–S–H gel) through the influence of anti-$Ca(OH)_2$-leaching. As a result, nano-filler enhanced the cement paste due to the high pozzolanic characteristic of NS.[39,41] The utilization of NS reduces the overall permeability due to the enhanced mechanical and durability properties of concrete.[22,37,42,43] Cost is a crucial issue in the construction industry. Although at a higher initial cost, the addition of small dosages of NS can be cost effective due to the enhanced mechanical and durability performance. Moreover, constructional workers could be exposed to nanomaterials, particularly by inhalation or dermal contact, during many operations like mixing, material handling, coating applications, and finishing operations.[44] Therefore, some precautions, such as ventilation of the area, wearing protective masks, gloves, and glasses, should be taken as safety procedures during a large number of construction operations.

Although there are several studies regarding ordinary SCC, there are a few or limited investigations related to the fresh and hardened state properties of SCAAC. Therefore, the research investigates the influences of combined utilization of nano-silica and steel fiber on the flowability, passing ability, and mechanical performances of GGBFS based SCAAC specimens cured at ambient environment. In addition, the sample thickness to steel fiber length (d/F_L) ratio is considered a significant parameter influencing the flexural strength and failure modes of the steel fiber reinforced concretes. In this research, the effects of two d/F_L ratios (3.33 and 1.25) on the failure modes of the steel fiber reinforced SCAAC specimens were studied, and cracking patterns were investigated in detail by considering steel fiber content, aspect ratio, and the existence of NS. Also, the relationship analyses between fresh and hardened state performance were conducted, and scanning electron microscope (SEM) analysis was carried out on a micro-scale.

Experimental methods

SCC ingredients

For the production of slag-based self-compacted alkali activated concretes (SCAAC), ground granulated blast furnace slag material was utilized with a specific gravity of 2.7 g/cm^3 and a specific surface area of 418 kg/m^2. In addition, the effect of nano-silica (NS) was investigated for the scope of the research. The specific surface and specific gravity of NS material were 150000 kg/m^2 and 2.2 g/cm^3.

The NS amount was utilized as 2% by weight of the GGBFS material. Table 1 indicates the chemical compositions and physical characteristics of NS and GGBFS. In addition, two types of steel fiber (SF1 and SF2) were utilized to investigate the effect of steel fibers on the mechanical strength of the SCAAC. For this purpose, two different steel fiber lengths and aspect ratios were used. The lengths were 30 mm and 60 mm; aspect ratios were 40 and 80 for SF1 and SF2, respectively. Three different steel fiber volumes (0.5%, 1%, and 1.5%) were utilized for each SCACC specimen.

For the SCACC production, ten different SCACC mixtures were designed using short and long fibrous specimens with V_f ratios of 0, 0.5%, and 1%, and NS ratios of 0% and 2%. The Master Glenium 51, a polycarboxylate-based superplasticizer, was utilized to obtain desired workability and flowability. The crushed stone with a maximum grain size of 16 mm and fine aggregates were utilized in the production of SCAAC. Table 2 presents the physical properties and the sieve analysis of the used aggregates. For the alkali activation of SCAAC mixes, a mixture of sodium silicate (SS) and 12 M sodium hydroxide (SH) was utilized with a SS/SH ratio of 2.5. As investigated in the earlier investigations, the optimum SS/SH ratio was found to be in the range of 1.5 to 2.5 for economic reasons.[45] Therefore, a SS/SH ratio of 2.5 was chosen in this research. The SS solution (SiO_2: 29.4%, water: 55.9%, and Na_2O: 13.7%, by weight) and the SH with a 97%–98% purity was commercially obtained from a local market. It was reported in the literature that the optimum SH molarity was 12 M[46] for better mechanical and durability performance of self-compacting AAC specimens; therefore, SH molarity was also selected as 12 M in this study.

Mix design

For the preparation of the slag-based SCACC specimens, two series were produced. One of the series was without nano-silica (NS0), and the other one involved 2% NS (NS2). Table 3 illustrates the used material amounts for 1 m^3 SCAAC specimens. The total binder amount was chosen as 500 kg/m^2. Steel fibers, SF1 (30 mm) and SF2 (60 mm length), were utilized with ratios of 0.5% and 1%. The steel fiber volume ratios of 0.5% and 1% were selected to obtain self-compacting concrete properties as indicated in the previous study.[47] The weight increases of steel fibrous specimens for 0.5% and 1% steel fiber volumes were 39 kg/m3 and 78 kg/m^3, respectively, which corresponds to 1.5% and 3% weight increases compared to non-fibrous specimens. Therefore, the weight increase due to the steel fiber incorporation should be considered in the structural design phases, resulting in higher lateral (earthquake) loads.

The characteristics of the self-compacting concrete are mainly influenced by binder type and amount, alkali activator type and content, maximum grain size

Table 1. The properties of the nanosilica and slag materials.

Materials	CaO	SiO_2	Al_2O_3	Fe_2O_3	MgO	SO_3	K_2O	Na_2O	Loss of ignition	Specific gravity	Blain fineness (m^2/kg)
NS (%)	–	99.80	–	–	–	–	–	–	<1.00	2.20	–
GGBFS (%)	34.12	36.40	11.39	1.69	10.30	0.49	3.63	0.35	1.64	2.79	418

Table 2. The sieve analysis and physical properties of aggregates.

Sieve size (mm)	16	8	4	2	1	0.5	0.25	Fineness modulus	Specific gravity	Absorption
Fine aggregate	100	100	100	67.3	39.9	28.40	16.4	2.57	2.45	1.5
Coarse aggregate	100	31.5	1	0.5	0.5	0.5	0.4	5.66	2.72	2.4

Table 3. Material amounts for the SCAAC mixes (kg/m^3).

Mixture	$Na_2SiO_3 + NaOH$	Slag	NS	SF	Fine aggregate	Coarse aggregate	Molarity (M)	SP (%)	Extra water (%)
0SF1NS0	250	500	0	0	860.07	738.12	12	7	10
0.5SF1NS0	250	500	0	39.2	860.07	738.12	12	7	10
1.0SF1NS0	250	500	0	78.4	860.07	738.12	12	7	10
0.5SF2NS0	250	500	0	39.2	860.07	738.12	12	7	10
1.0SF2NS0	250	500	0	78.4	860.07	738.12	12	7	10
0SFNS2	250	490	10	0	858.49	736.76	12	7	10
0.5SF1NS2	250	490	10	39.2	858.49	736.76	12	7	10
1.0SF1NS2	250	490	10	78.4	858.49	736.76	12	7	10
0.5SF2NS2	250	490	10	39.2	858.49	736.76	12	7	10
1.0SF2NS2	250	490	10	78.4	858.49	736.76	12	7	10

(D_{max}), steel fiber volume fraction, and steel fiber aspect ratio. In addition, it was found in the earlier investigation that mechanical properties of the steel fibrous SCC specimens are also influenced by sample thickness/steel fiber length ratio (d/F_L).[47]

During mixing, dry ingredients (binder and aggregates) were mixed for 2 min. Then, the superplasticizer, extra water, and alkali activators were added into the mixer in one minute and mixed for 2 min. Finally, the SCAAC mixture was further mixed for 3 min to obtain a uniform and homogeneous mixture.

The fresh properties tests of SCAAC mixes

The fresh state tests; L-box test, V-Funnel test, slump flow diameter, and slump flow time (T_{50}) were conducted to check the requirements of passing ability and flowability properties of the steel fiber reinforced SCAAC mixes by EFNARC committee.[48] The L-Box test measured the passing ability, flowability and viscosity were measured via slump flow and V-funnel tests. For slump flow tests, flow dimensions along both x and y directions were measured, and T_{50} time, that flow dimension arrives at 50 cm, was recorded. Meanwhile, SCAAC mixes were poured into the V-Funnel section, and the discharge duration from the V-funnel section was recorded. The passing ability between narrower openings was measured via the L-box test. The ratio of the lateral section height to vertical section height (PL value) yields the passing ability value of the fresh mixes.

Curing conditions

After casting of the specimens, the top face of the samples was coated with a plastic sheet to hinder alkali activator evaporation. Then, the SCAAC samples were demolded 24 h later and put in the laboratory medium at $23 \pm 2°C$ for 28 days. The previous investigation reported that slag-based alkali-activated concretes can be utilized in structural applications without oven-curing or water curing.[49] Therefore, oven-curing or water curing was not applied to the specimens.

The hardened properties

The compressive strength tests were executed to evaluate the effects of steel fiber and nano-silica utilization together with the strengths of SCAAC samples. The 100 mm × 100 mm × 100 mm cubic SCAAC samples were produced to obtain compressive strength values by ASTM C39 standard.[50] In addition, 100 mm × 200 mm cylinder specimens were used to evaluate both elasticity modulus and splitting tensile strength of the SCAAC specimens according to ASTM C496 standard. The upper surface of the cylinder specimens was capped with sulfur by ASTM C617 to obtain a smooth surface before loading. Moreover, four-point flexural tensile strength tests were executed on 100 mm × 100 mm × 500 mm fiber-reinforced SCAAC prismatic specimens via displacement-controlled loading with a rate of 0.02 mm/min. Three linear variable displacement transducers (LVDT) were used to evaluate the deflection of specimens.

Result and discussions

The fresh properties of SCAAC

Table 4 summarizes the fresh state properties of the SCAAC specimens. The results indicated that minimum flowability was obtained at 659 mm for the 1.0SF2NS0 mixtures, which satisfied the minimum flowability requirements of EFNARC specification (550 mm)[48] and EN 12350-8 standard (600 mm).[51] The PL value should be higher than 0.8 according to the indicated regulation/standard for the L-box tests. The results showed that all PL values of the SCAAC mixes were found higher than 0.8, satisfying the required passing ability. Regarding the V-funnel test, the discharge duration is allowed to be a maximum of 15 s to achieve excellent filling properties. The results indicated that non-fibrous and 0.5 steel fibrous specimens (approximately) satisfied this criterion. However, for further steel fiber inclusion (1%), the discharge time was higher than 15 s, and it was 24 s (maximum) for the 1.0SF2NS0 specimens. However, no blocking was observed for 1% steel fiber reinforced SCAAC mixtures. The standard[48] suggests that the T_{50} duration of the mixes should be lower than 6 s for the high flowability of the self-compacting mixes. The results indicated that the T_{50} duration of all SCAAC mixes satisfied the criterion of 6 s, indicating that SCAAC mixes have adequate flowability characteristics.

Table 4. The fresh state properties of SCAAC mixtures.

Mixture	Slump flow (mm)	L-box	V-funnel	T_{50}
0SF1NS0	741	1	10.71	2.46
0.5SF1NS0	707	0.96	14.25	3.13
1SF1NS0	664	0.83	19.91	3.63
0.5SF2NS0	693	0.94	17.09	3.37
1SF2NS0	659	0.81	23.49	4.07
0SFNS2	750	1	9.25	2.21
0.5SF1NS2	720	0.97	13.88	2.87
1SF1NS2	687	0.85	18.33	3.59
0.5SF2NS2	710	0.96	16.62	3.23
1SF2NS2	661	0.82	22.61	3.97

The effects of NS and SF type and amounts on flowability. Figure 1 indicates the slump flow values for each different mix. The results indicated that 2% NS addition slightly improved the slump flow values. However, the slump flow of the mixes reduced with an increase in the steel fiber content. The 1% steel fiber reinforced SCAAC specimens exhibited poor performance. In addition, the slump flow of the SCAAC mixes reduced with an increase in the length of SF and aspect ratios. The long steel fiber (60 mm) reinforced SCAAC mixes

(SF2) showed slightly more poor flowability performance than the short steel fiber (30 mm) reinforced SCAAC mixes. The measured slump flow values were in the range of the values of EFNARC specification.[48] Therefore, it can be concluded that the SCAAC mixes are suitable for structural applications like columns, beams, and slabs.

Effects of nanosilica and steel fiber on $T5_0$ duration. Figure 2 shows the T_{50} durations of the SCAAC mixes. The lowest T_{50} duration was obtained from the specimens without SF and 2% NS, indicating the highest flowability. The T_{50} duration increased with the further SF amounts (1%). Furthermore, T_{50} duration was more of long steel fiber (60 mm) reinforced specimens than short steel fiber (30 mm) reinforced specimens. The highest T_{50} duration and the lowest flowability were obtained from the 1SF2NS0 specimens. In general, similar results were obtained with the slump flow values regarding T_{50} durations.

Effects of steel fibers and nanosilica on V-funnel flow. Figure 3 (a) shows the V-funnel discharge durations of SCAAC mixes. The lowest V-funnel discharge time was obtained for the specimens with NS and without steel

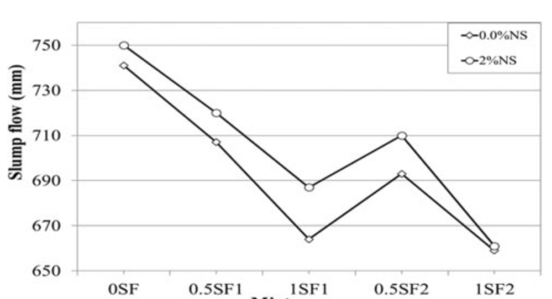

Figure 1. The effect of nanosilica and steel fiber lengths and amounts on the flowability results of SCAAC.

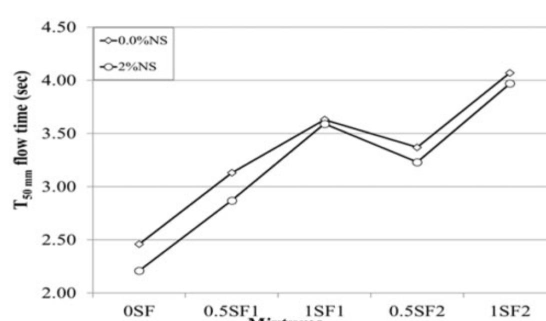

Figure 2. The influences of steel fiber and nanosilica on T50 duration of the SCAAC.

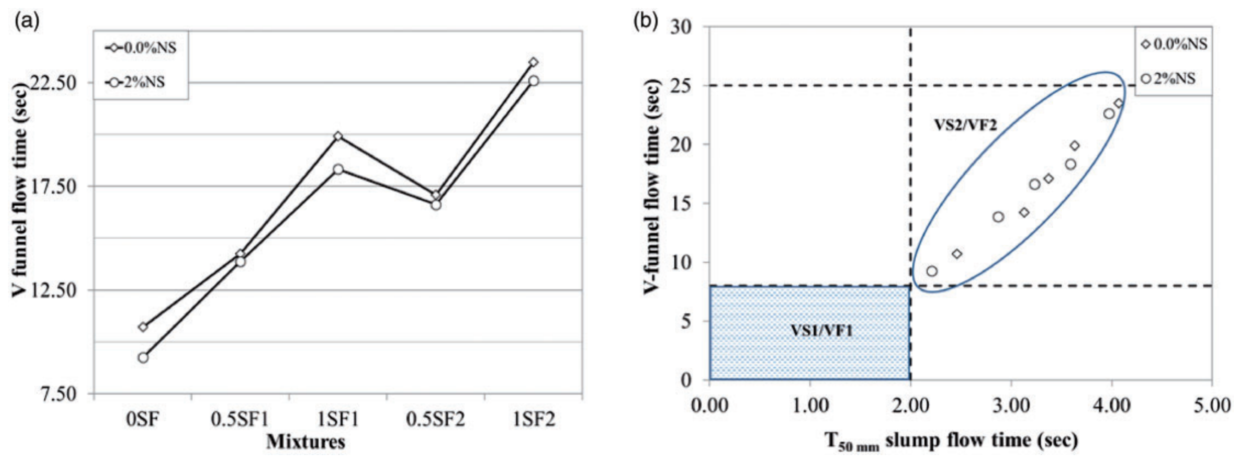

Figure 3. The combined effect of SF and NS on the V-funnel time (a), T_{50} flow time vs V-funnel relationships (b). (a) The effect of SF and NS on V-funnel duration. (b) V-funnel versus T_{50} flow time.

fiber, while the highest discharge time was recorded for the specimens without NS and with 2% SF.

Similar to slump flow and T_{50} duration, V-funnel discharge time also increased with an increase in the steel fiber volume ratio (1%). In addition, specimens, including 60 mm steel fibers (SF2) showed higher V-Funnel discharge duration than the specimens, including 30 mm steel fibers (SF1), indicating that longer fibers and higher aspect ratios caused a decrease in flowability. Similar results were also obtained from SCC specimens in the previous study.[52]

Figure 3(b) presents V-funnel discharge duration and T_{50} flow duration relationships. The obtained results indicated that all SCAAC mixes were in the region of VS2/VF2 classification,[48] which has a low formwork pressure and good resistance to segregation and bleeding.

Effects of steel fiber and nanosilica on the L-box test. The L-Box represents the passing ability of SCAAC mixtures through the tight spacings (41 ± 1 mm). The passing ability was measured by dividing the horizontal height of mixes to the vertical height of the mixes (H_2/H_1). For the passing ability criteria, the H_2/H_1 ratio should be above the ratio of 0.8 according to the related regulations/standards. Figure 4 presents the L-box test results for the SCAAC mixes. The superior passing ability was obtained in the specimens without steel fibers, whereas poor performance was observed for the specimens, including 1% long steel fiber (SF2). The passing ability of the SCAAC mixtures reduced as the steel fiber volume ratio (V_f) increased in the SCAAC mixes. In addition, the higher steel fiber length and aspect ratio decreased the passing ability of the SCAAC mixes. The NS addition slightly improved the passing ability properties of the SCAAC mixes.

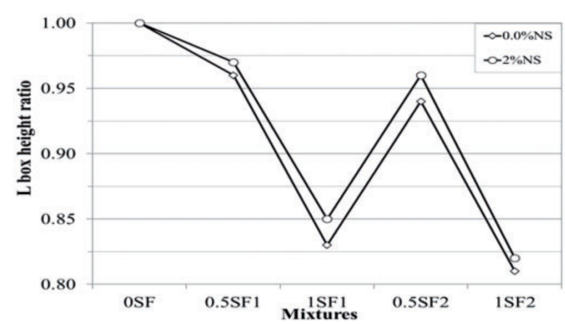

Figure 4. The variation of the L-Box ratio with SF and NS contents.

Therefore, the incorporation of NS into the SCAAC mixes is recommended to achieve superior fresh state properties.

Hardened state performance of SCAAC specimens

Compressive strength. Figure 5 shows the specimens before and after compressive strength tests. The cube specimens were loaded under uniaxial compressive stresses with a loading rate of 0.6 MPa/s. Table 5 and Figure 6 illustrate the hardened state performance and compressive strength values of the SCAAC specimens, respectively. The results pointed out that NS addition slightly decreased the compressive strengths of the SCAAC samples. It may be attributed to the unreacted NS particles that cause self-dehydration and cracks in the matrix, reducing compressive strengths of the samples.[38,53]

Meanwhile, the steel fiber addition enhanced the compressive strength of the SCAAC samples. The compressive strength improvement was obtained as 5% and 9% for SF 1 and SF2 specimens with a steel fiber ratio of 0.5%, respectively. In comparison, the improvement

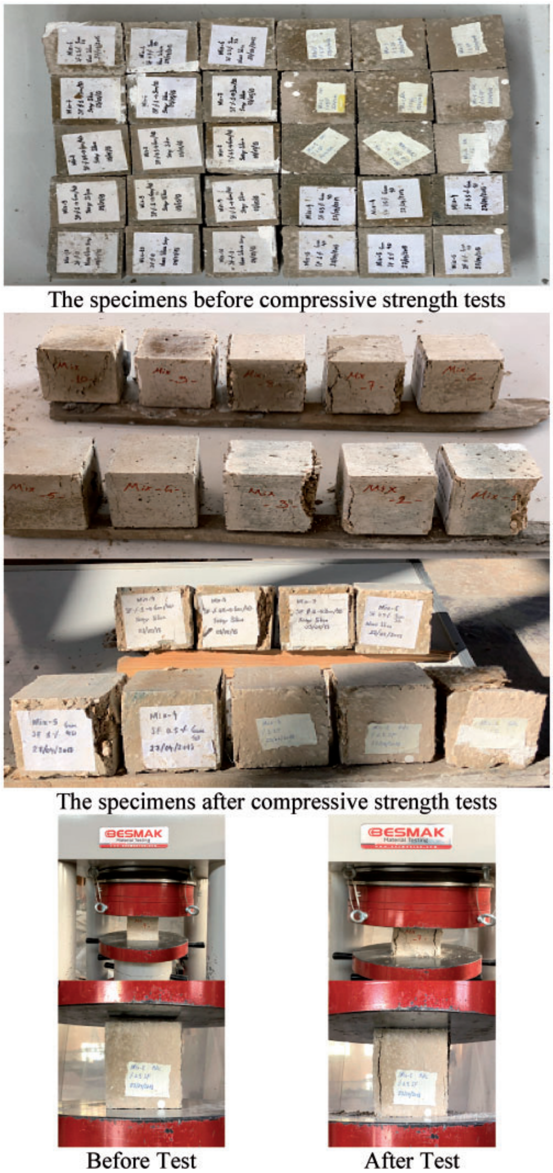

Figure 5. The specimens before and after compressive strength tests.

was 9% and 13% for SF1 and SF2 specimens with a steel fiber ratio of 1%, respectively. The compressive strength improvement due to the steel fiber inclusion was also found in the earlier investigations.[54,55] Meanwhile, the obtained results also indicated that the higher steel fiber aspect ratio (80) also increased compressive strengths of the SCAAC samples, and the highest compressive strength was obtained for the 1% long steel fibrous (high aspect ratio) SCAAC specimens without NS (1SF2NS0). The favorable effect of a high aspect ratio on the compressive strength of the specimens was also reported in the earlier investigations.[56–58]

Modulus of elasticity. Table 5 presents the modulus of elasticity test results of the cylindrical specimens. The results indicated that the modulus of elasticity was in the range of 20.49 GPa to 33.11 GPa for slag-based SCAAC specimens. The highest elasticity modulus was obtained fromr the 1SF2NS0 specimens, while the lowest elasticity modulus was obtained from the 0SF1NS2 specimens, indicating similarity with compressive strength test results. Moreover, the influence of nano-silica and steel fiber on the modulus of elasticity results was similar to the effects on compressive strength results. It was found that the NS incorporation decreased the modulus of elasticity results of the specimens, which may be attributed to unreacted NS particles in the matrix.

Splitting tensile strength. Figure 7 illustrates the variation of splitting tensile strength results of cylindrical SCAAC specimens with and without NS and SF. The results indicated that the splitting tensile strength of SCAAC specimens increased with an increase in SF content and aspect ratio. The splitting tensile strength values increased about 39% for 1SF1NS0 and 62% for 1SF2NS0 specimens with respect to splitting tensile strengths of non-fibrous specimens. The favorable

Table 5. Hardened state properties of SCAAC specimens.

Mixtures	Steel fiber aspect ratio	Steel fiber volume fraction	NS%	Comp. strength (MPa)	Mod. of elasticity (GPa)	Splitting tensile strength (MPa)	Max. load (KN)	Net flexural strength (MPa)	Disp. (mm)
0SF1NS0	0	0	0%	60.95	20.73	3.43	8.65	3.89	0.82
0.5SF1NS0	40	0.5	0%	64.30	22.15	3.92	8.77	3.94	23.00
1.0SF1NS0	40	1.0	0%	66.93	29.09	4.76	10.25	4.61	31.00
0.5SF2NS0	80	0.5	0%	66.52	24.39	4.36	9.10	4.10	30.50
1.0SF2NS0	80	1.0	0%	69.08	33.11	5.55	13.67	6.15	40.00
0SF1NS2	0	0	2%	59.73	20.49	3.29	7.96	3.58	1.12
0.5SF1NS2	40	0.5	2%	61.41	23.25	4.90	8.86	4.03	27.00
1.0SF1NS2	40	1.0	2%	62.53	26.65	5.42	10.93	4.92	37.00
0.5SF2NS2	80	0.5	2%	62.72	23.62	5.62	12.23	5.50	37.25
1.0SF2NS2	80	1.0	2%	66.12	31.41	6.32	14.67	6.60	46.30

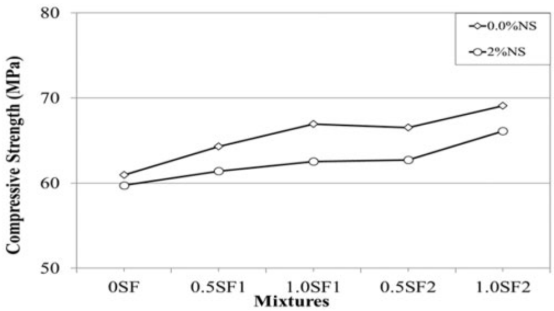

Figure 6. The influence of steel fiber and nanosilica on the compressive strength results of SCAAC samples.

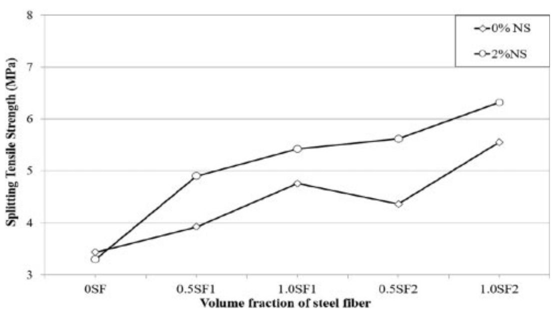

Figure 7. The effect of steel fiber and nanosilica on the splitting tensile strengths of SCAAC specimens.

influence of steel fibers on the splitting tensile strength was also reported in earlier studies.[59–62] For the lower steel fiber inclusion (0.5%), the splitting tensile strength of the specimens also increased at a decreasing rate. In addition, increases in the splitting tensile strength values were found 58% for 1SF1NS2 and 84% for 1SF2NS2 specimens. The results pointed out that the 2% NS utilization also enhanced the splitting tensile strength test results, and this improvement was found to be higher for the fiber reinforced specimens with a higher aspect ratio. This improvement may be attributed to the dense microstructure and excellent bond strength between matrix and steel fibers in the presence of NS. However, when steel fibers were not utilized in the SCAAC specimens, similar splitting tensile strength results were obtained from the specimens without NS and 2% NS. The result pointed out that for the steel fibrous specimens, NS utilization, enhanced the tensile strength properties of the SCAAC samples. It was reported in the earlier investigation that modulus of elasticity, compressive and splitting tensile strengths were influenced by the concrete quality.[63] In this study, the adverse effect of NS was compensated by steel fiber since the steel fibers arrested emerged cracks. The combined use of steel fiber and NS in the 50% fly ash and 50% slag based geopolymer specimens was investigated in the earlier investigation. It was found that SF had no favorable effect on compressive strength. However, a significant effect was found on bending and bond strengths.[35]

The four-point bending tests for SCAAC specimens. Figure 8 illustrates the load vs. displacement curves of the different SCAAC specimens under four-point bending tests. The maximum load and displacement values are also given in Table 5 for upcoming model studies. A linear slope was observed up to the first crack in the pre-peak zone, and then strain-softening was observed in the post-peak zone during four-point bending tests for all SCAAC specimens. In Figure 8(a) and b, the influences of SF on SCAAC specimens with and without NS are shown. The results indicated that the flexural strength of the steel fibrous SCAAC specimens enhanced with an increase in the steel fiber ratio. Also, flexural strengths of the NS incorporating specimens were found higher than the strengths of the specimens without NS. A similar result was also obtained for the 50% fly ash and 50% slag based AAC specimens in the earlier investigation.[35]

In addition, the sharp decrease in the post-peak zone decreased for the specimens, including NS (Figure 8(a)) as compared to the specimens without NS (Figure 8(b)) regarding steel fibrous SCAAC specimens. Furthermore, the flexural performance of specimens with a higher aspect ratio (SF2) was better than the specimens with a low aspect ratio (SF1). For the specimens with NS post-peak performance of 0.5% steel fibrous specimens with a higher aspect ratio was found to be better than the 1% steel fibrous specimens with a lower aspect ratio as shown in Figure 8(a). For the specimens without NS, the flexural performance was influenced by the steel fiber ratio, and it can be concluded that the higher the steel fiber ratio, the better flexural performance, as shown in Figure 8(b). The enhanced flexural performance may be attributed to the improved interfacial transition zone and higher bond strength between NS particles and steel fibers, especially for higher aspect ratio. The favorable influences of steel fiber on tensile strength,[64,65] flexural strength and failure performance,[55] and bond strength[35] were also found in the previous studies. In another study, the effect of different steel fiber aspect ratios was studied, and tensile strength and fracture toughness were found to be high for the specimens with high steel fiber aspect ratio.[36] In addition, when Figure 8(c) and (d) were investigated, the more toughness and controlled load decrease obtained from the specimens including NS. Meanwhile, for the non-fibrous specimens, similar load-deflection curves were obtained as shown in Figure 8(e), proving that nanosilica utilization became significant when it was utilized with steel fibers in the SCAAC specimens.

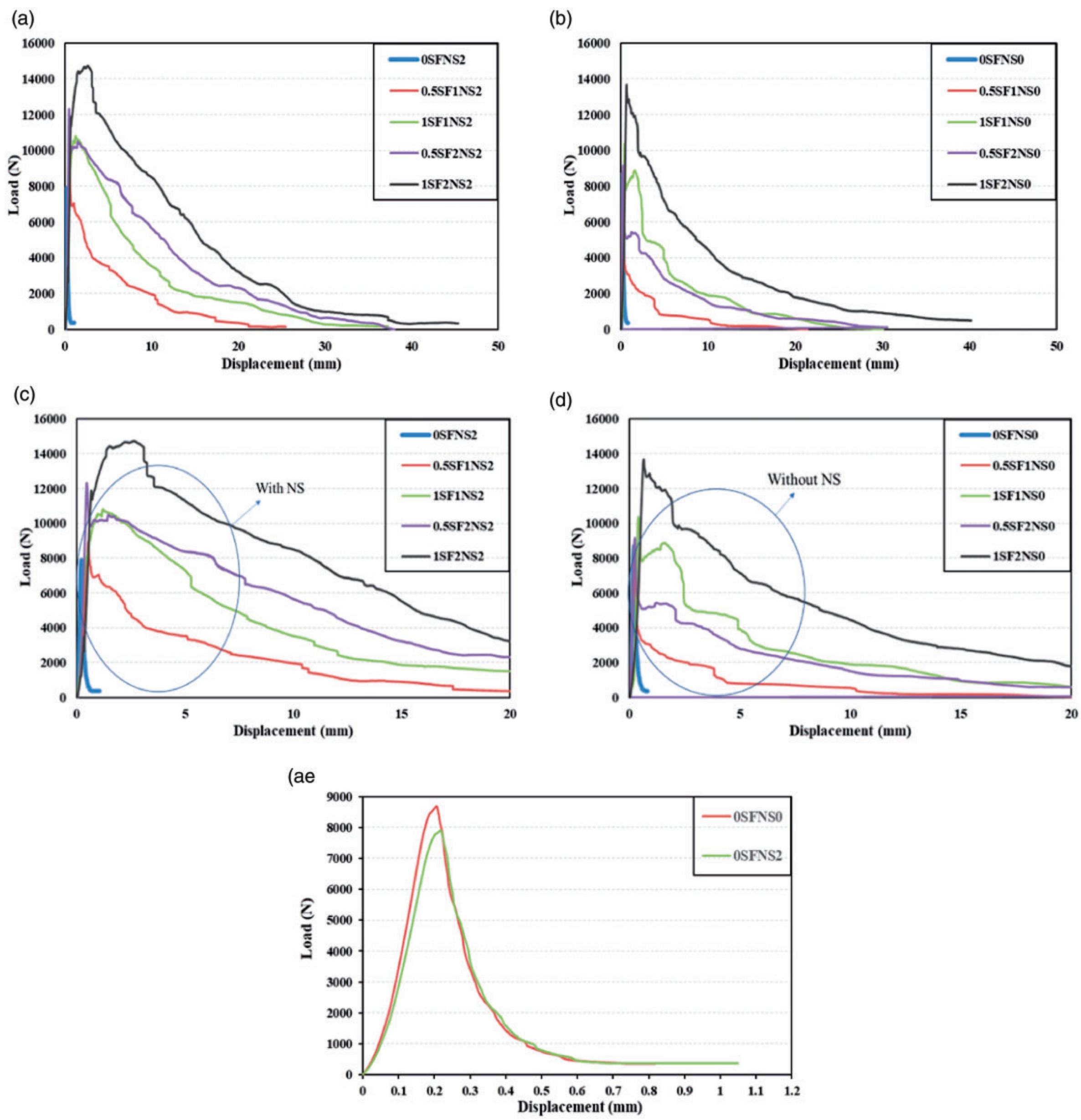

Figure 8. Load vs displacement curves of SCAAC specimens under four-point bending. (a) Effect of SF on SCAAC mixes with NS. (b) Effect of SF on SCAAC mixes without NS. (c) Effect of SF on SCGC mixes with NS in detail. (d) Effect of SF on SCGC mixes with NS in detail. (e) Effect of NS on SCGC mixes without SF.

Failure modes of the SCAAC specimens under flexure

Figure 9 illustrates the cracking patterns of SCAAC specimens before (a) and after (b) failure. The crack pattern photos of the specimens were given for both non-fibrous and 1% steel fiber reinforced self-compacting alkali-activated concrete (SCAAC) specimens. The results indicated that cracking patterns were influenced by the existence of nano-silica and steel fiber. The crack arresting capability of fibers can be represented by the sample thickness/steel fiber length ratio (d/F_L ratio).[50] The efficiency of SF increased when the d/F_L ratio decreased. For the low d/F_L ratios, steel fibers can arrest the cracks easily. The sudden failure occurred in the middle of the specimens without NS and SF, as shown in Figure 9(a) and (b). For the 1SF1NS0 specimens (without NS), a single enormous crack with a wider size occurred in the maximum moment zone (flexure crack) without hairline crack, as shown in Figure 9(c) and (d). The d/F_L ratio was 3.33 for these specimens, and the steel fiber efficiency was found to be less due to the single and

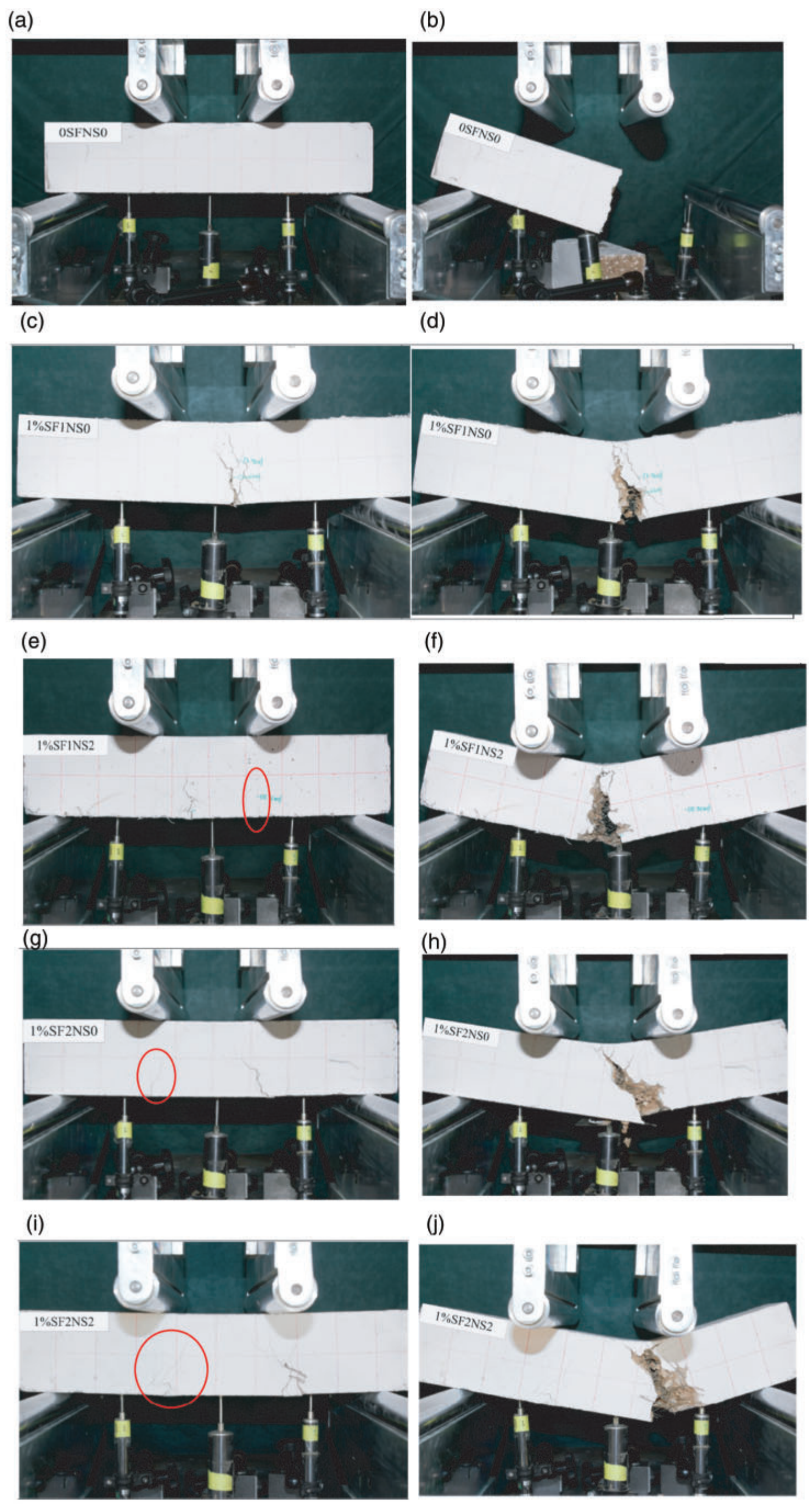

Figure 9. Failure modes of SCAAC specimens with and without NS and SF. (a) SCAAC specimen without NS & SF before failure. (b) SCGC specimen without NS & SF after failure. (c) SCAAC specimen without NS & with 1%SF1 before failure. (d) SCGC specimen without NS & with 1%SF1 after failure. (e) SCGC specimen with NS & 1%SF1 before failure. (f) SCGC specimen with NS & 1%SF1 after failure. (g) SCGC specimen without NS & with 1%SF2 before failure. (h) SCGC specimen without NS & with 1%SF2 before failure. (i) SCGC specimen with NS & 1%SF2 before failure. (j) SCGC specimen with NS & 1%SF2 after failure.

wide crack, and the crack was found to be parallel to the loading direction. For the 1SF1NS2 specimens (with 2% NS), the main crack formed again in the bending zone (flexure crack). However, an additional hairline crack, with a size of 1 mm, formed prior to failure as shown with the red circle in Figure 8(e). For this case (d/F_L:3.33), the main failure crack formed with a lower width and parallel to the loading direction. For the 1%SF2NS0 (d/F_L:1.25) specimens, the inclined crack (45°) formed around the support, not located in the middle. Moreover, an additional inclined crack formed with a wider size (>1 mm) that emerged around the supports. For the SCAAC samples having a d/F_L ratio of 1.25, the failure was realized from the flexural-shear type of cracks. For the 1%SF2NS2 (d/F_L:1.25) specimens with NS, multiple branching type of cracks formed in bending zone, but main cracks proceeded to the failure were found to be inclined with a wider crack width at support zone. Additional multiple inclined hairline cracks were also observed around support. The main failure crack type was observed as a flexural-shear type of crack for the SCAAC samples having a d/F_L ratio of 1.25. The inclined and multiple cracks around supports were attributed to the stress transfer among the steel fibers. This stress transfer by steel fibers was found more when the d/F_L ratio was low since specimens can arrest the cracks easily for small d/F_L ratios, enabling stress transfer via multiple long steel fibers. Furthermore, the NS enhanced the bond between matrix and steel fibers, enabling improved flexural performance.

Relationship and correlation between hardened and fresh state

In order to evaluate the experimental results, it is significant for a researcher to find the correlation between the experimental data. As stated earlier, the mechanical characteristic of the concrete was substantially affected by the compressive strength values of concrete. In this research, correlations between the fresh state properties and hardened state properties were investigated. The close relationships were observed between T_{50} flow time and slump flow (R^2: 0.9127), slump flow and L-Box (R^2: 0.914), and slump flow and V-funnel results (R^2: 0.956) as indicated in Figure 10(a) to (c), respectively.

In addition, the relationships between slump flow and the mechanical properties of SCAAC specimens were also investigated and illustrated in Figure 11. The results indicated strong relationships among compressive strength-slump flow, splitting tensile strength-slump flow, modulus of elasticity-slump flow, and flexural strength-slump flow, as shown in Figure 11 (a) to (d). The R^2 results also showed that stronger

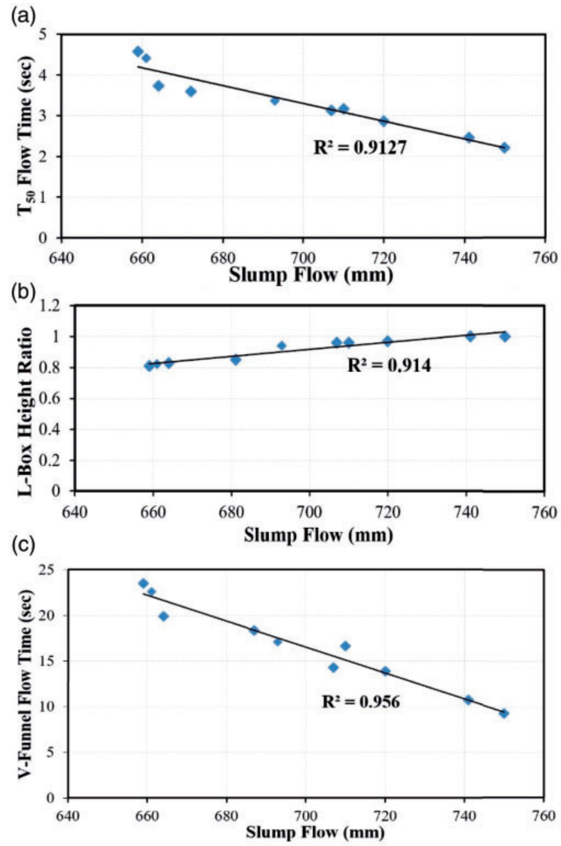

Figure 10. Correlations between the fresh state properties. (a) T_{50} duration versus slump flow. (b) L-Box versus slump flow. (c) V-Funnel versus slump flow.

relationships were observed for the specimens with 2% NS compared to specimens with NS. The obtained findings pointed out that the mechanical performance of specimens was directly related to the slump flow of the SCAAC mixes, which can be attributed to the increased steel fiber orientations in the casting directions with higher flowability, resulting in improved mechanical performance.

Scanning electron microscopy analysis

Figure 12 illustrates the scanning electron microscopy (SEM) of the SCAAC specimens with/out NS to identify the influence of NS on the interfacial transition zone (ITZ). Figure 12(a) and (b) show the non-fibrous specimens with/out NS. The results showed that the microstructure of specimens with NS showed fewer pores and dense microstructure (Figure 12(b)) compared to the microstructure of specimens without NS (Figure 12(a)). However, more micro cracks were found in the microstructure of the SCAAC specimens with NS (Figure 12(d)), resulting in lower compressive strength for the NS incorporating specimens. For the specimens without NS, less micro cracks were

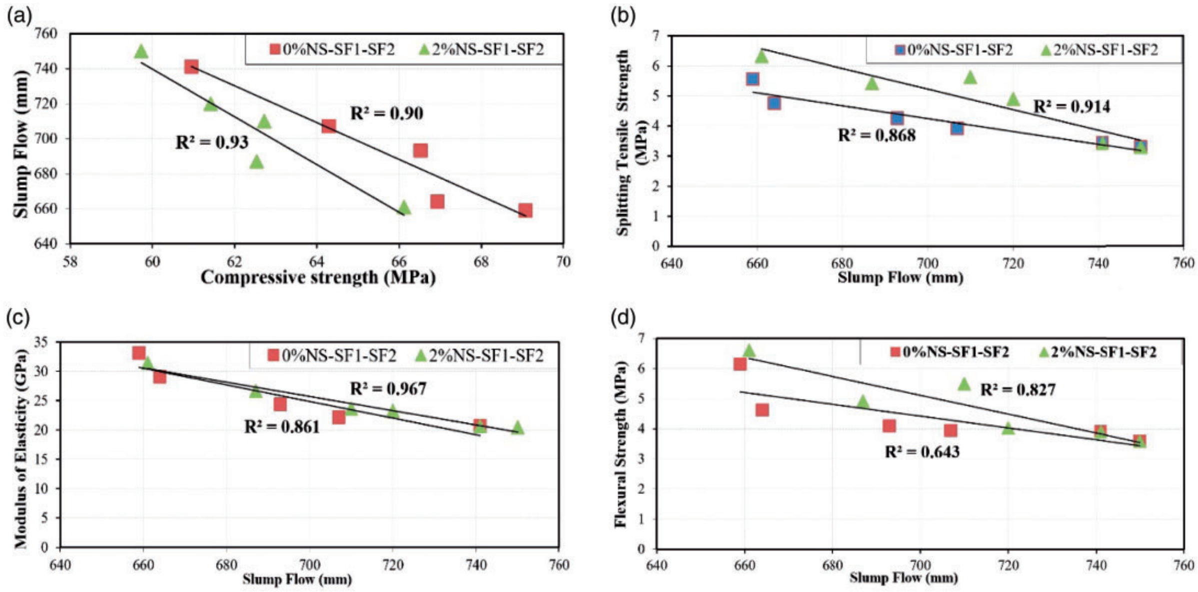

Figure 11. Correlation between the hardened and fresh properties of SCAAC. (a) Compressive strength vs slump flow. (b) Splitting tensile strength vs slump flow. (c) Modulus of elasticity vs slump flow. (d) Flexural strength vs slump flow.

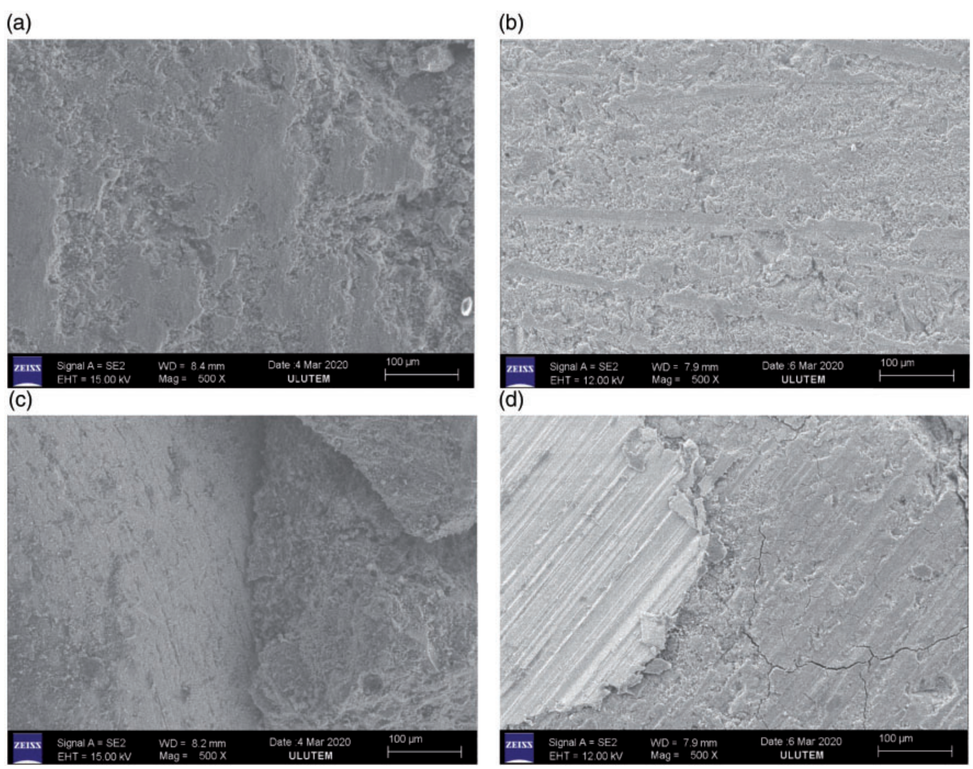

Figure 12. SEM images of SCAAC with and without NS with different scales. (a) Specimens without SF and NS. (b) Specimens without SF and with 2% NS. (c) Specimens with 1% SF1 and without NS. (d) Specimens with 1% SF1 and with 2% NS.

observed, as shown in Figure 12(c), causing the improved compressive strength of the specimens. Meanwhile, more reaction products were observed between steel fibers and matrix at ITZ in the microstructure of specimens with NS (Figure 12(d)), which may be attributed to improved bond strength between steel fibers and matrix, resulting in the enhanced flexural performance of steel fibrous specimens with NS. Similar observations that denser microstructure and improved bond strength are also reported in the earlier investigations.[22,66,67]

Conclusions

In the scope of the research, the fresh state and hardened state performance of slag based ambient-cured self-compacting alkali activated concrete (SCAAC) specimens with/out nano-silica (NS) was investigated. In addition, the influence of steel fibers (SF) with two different volumes (0.5% and 1%) and aspect ratios (40, 80) on the both fresh and mechanical properties was evaluated. In addition, the influence of sample thickness/steel fiber length ratio (d/F_L) on the flexural performances and failure modes of the SCAAC specimens was investigated. The following conclusions were obtained;

- The passing ability and flowability of the SCAAC mixes decreased with an increase in both steel fiber content and aspect ratio. The specimens with 1% steel fiber and aspect ratio of 80 and without nano-silica (1SF2NS0) exhibited the poorest flowability and passing ability.
- The NS utilization enhanced the passing ability and flowability, and the nano-silica compensated the adverse effect of steel fibers on flowability and passing ability.
- The flowability and passing ability tests (slump flow, T_{50}, V-funnel, V-funnel, and L-box) indicated that all SCAAC mixes had adequate requirements of flowability and passing ability according to the limitations of the related guidelines/standards.
- The compressive strength and elasticity modulus of specimens increased with an increase in both SF volume and aspect ratio but decreased with the inclusions of NS. The 1SF2NS0 SCAAC specimens had the highest compressive strength and modulus of elasticity.
- The flexural strengths and splitting tensile strengths enhanced with an improvement in both SF volumes and aspect ratios. Also, NS enhanced the splitting tensile and flexural strength results. The enhanced performance due to NS may be attributed to the improved interfacial transition zone and higher bond strength between NS and SF, especially for the higher SF aspect ratios. The superior tensile and flexural strengths were obtained from the 1SF2NS2 specimens.
- The sample thickness/steel fiber length ratio (d/F_L) was found a significant parameter in addition to the SF volume and aspect ratio on the failure modes of the SF reinforced SCAAC specimens under the bending test. The specimens having a d/F_L ratio of 3.33 showed flexural cracks in the middle of the specimens, whereas the specimens having a d/F_L ratio of 1.25 exhibited inclined flexural-shear cracks at the bending zone around the supports especially for specimens with 1% steel fiber volume. The SF efficiency was found more with a decrease in d/F_L ratio since crack arresting capability improved as d/F_L ratios decreased.
- The NS also affected the failure modes of the specimens by improving the bond strength between SF and matrix so that stress transfer can be possible and the cracks further extend from bending zone to shear zone by SF depending on the d/F_L ratio and SF content.
- Strong relationships were observed between T_{50} flow time and slump flow (R^2: 0.9127), slump flow and L-Box (R^2:0.914), and slump flow and V-funnel results (R^2:0.956). Also, close relationships were obtained between the slump flow and mechanical properties of SCAAC specimens. This can be attributed to the increased SF orientations along the casting direction with higher flowability, resulting in improved mechanical performance.
- The SEM microstructure of specimens with NS showed fewer pores and dense microstructure with respect to specimens without NS. In addition, more reaction products were observed between SF and matrix at ITZ in the microstructure of specimens with NS, which may be attributed to improved bond strength between SF and matrix, resulting in enhanced tensile and flexural performance. However, more micro cracks were found in the microstructure of NS incorporating specimens, resulting in a decrease in the compressive strength of the specimens.
- The SF reinforced SCAAC specimens can be utilized for structural applications.

Declaration of Conflicting Interests

The author(s) declared no potential conflicts of interest with respect to the research, authorship, and/or publication of this article.

Funding

The author(s) disclosed receipt of the following financial support for the research, authorship, and/or publication of this article: This work was supported by Gaziantep University Scientific Research Projects Coordination Unit. Project number: MF.DT.17.06.

ORCID iDs

Radhwan Alzeebaree https://orcid.org/0000-0003-2496-3322
Anıl Niş https://orcid.org/0000-0001-9092-8088
Mehmet Eren Gülşan https://orcid.org/0000-0002-8991-0363

References

1. Pierrehumbert R. There is no plan B for dealing with the climate crisis. *Bull Atom Sci* 2019; 75: 215–221.
2. Garg A and Singhal D. Review on the durability properties of sustainable alkali activated concrete. *Mater Today: Proc* 2020; 33: 1643–1649.
3. Hardjito D and Rangan BV. Development and properties of low-calcium fly ash-based geopolymer concrete. 2005. http://hdl.handle.net/20.500.11937/5594
4. Rangan BV. Low-calcium, fly-ash-based geopolymer concrete. In: Nawy EG (ed.) *Concrete construction engineering handbook*. Boca Raton, FL: Taylor and Francis Group, 2008, 26, pp, 1–29.
5. Temuujin J, van Riessen A and MacKenzie KJD. Preparation and characterisation of fly ash based geopolymer mortars. *Constr Build Mater* 2010; 24: 1906–1910.
6. Kong DLY and Sanjayan JG. Damage behavior of geopolymer composites exposed to elevated temperatures. *Cem Concr Compos* 2008; 30: 986–991.
7. Wang A, Zheng Y, Zhang Z, et al. The durability of alkali-activated materials in comparison with ordinary Portland cements and concretes: a review. *Engineering* 2020; 6: 695–706.
8. Amran YM, Alyousef R, Alabduljabbar H, et al. Clean production and properties of geopolymer concrete; a review. *J Clean Prod* 2020; 251: 119679.
9. Hardjito D, Wallah SE, Sumajouw DMJ, et al. On the development of fly ash-based geopolymer concrete. *Mater J* 2004; 101: 467–472.
10. Nazari A and Sanjayan JG. Modelling of compressive strength of geopolymer paste, mortar and concrete by optimized support vector machine. *Ceram Int* 2015; 41: 12164–12177.
11. Pacheco-Torgal F, Abdollahnejad Z, Miraldo S, et al. *Alkali-activated cement-based binders (AACBs) as durable and cost-competitive low-CO_2 binder materials: some shortcomings that need to be addressed*. Oxford: Butterworth-Heinemann, 2017, pp.195–216.
12. Ghezal A and Khayat KH. Optimizing self-consolidating concrete with limestone filler by using statistical factorial design methods. *Mater J* 2002; 99: 264–272.
13. Khayat KH. Optimization and performance of air-entrained, self-consolidating concrete. *Mater J* 2000; 97: 526–535.
14. Khayat KH, Paultre P and Tremblay S. Structural performance and in-place properties of self-consolidating concrete used for casting highly reinforced columns. *Mater J* 2001; 98: 371–378.
15. Felekoğlu B, Türkel S and Baradan B. Effect of water/cement ratio on the fresh and hardened properties of self-compacting concrete. *Build Environ* 2007; 42: 1795–1802.
16. Ferraris CF, Brower L, Ozyildirim C, et al. Workability of self-compacting concrete. In: *Symposium proceedings of PCI/FHWA/FIB international symposium on high performance concrete: the economical solution for durable bridges and transportation structures*, Orlando, FL, USA, 25–27 September 2000.
17. Xie J, Wang J, Rao R, et al. Effects of combined usage of GGBS and fly ash on workability and mechanical properties of alkali activated geopolymer concrete with recycled aggregate. *Compos Part B Eng* 2019; 164: 179–190.
18. Noushini A, Aslani F, Castel A, et al. Compressive stress-strain model for low-calcium fly ash-based geopolymer and heat-cured Portland cement concrete. *Cem Concr Compos* 2016; 73: 136–146.
19. Kurtoğlu AE, Alzeebaree R and Aljumaili O. Mechanical and durability properties of fly ash and slag based geopolymer concrete. *Adv Concr Constr* 2018; 6: 345.
20. Zhang P, Zheng Y, Wang K, et al. A review on properties of fresh and hardened geopolymer mortar. *Compos Part B Eng* 2018; 152: 79–95.
21. Khaloo A, Raisi EM, Hosseini P, et al. Mechanical performance of self-compacting concrete reinforced with steel fibers. *Constr Build Mater* 2014; 51: 179–186.
22. Alzeebaree R, Çevik A, Nematollahi B, et al. Mechanical properties and durability of unconfined and confined geopolymer concrete with fiber reinforced polymers exposed to sulfuric acid. *Constr Build Mater* 2019; 215: 1015–1032.
23. Tamil Selvi M and Thandavamoorthy TS. Mechanical and durability properties of steel and polypropylene fibre reinforced concrete. *Int J Earth Sci Eng* 2014; 7: 696–703.
24. Gencel O, Brostow W, Datashvili T, et al. Workability and mechanical performance of steel fiber-reinforced self-compacting concrete with fly ash. *Compos Interfaces* 2011; 18: 169–184.
25. Frazão C, Camões A, Barros J, et al. Durability of steel fiber reinforced self-compacting concrete. *Constr Build Mater* 2015; 80: 155–166.
26. Ahmed Memon F, Nuruddin MF, Demie S, et al. Effect of curing conditions on strength of fly ash-based self-compacting geopolymer concrete. *Int J Civ Environ Eng* 2011; 3: 183–186.
27. Ahmed MF, Nuruddin MF and Shafiq N. Compressive strength and workability characteristics of low-calcium fly ash-based self-compacting geopolymer concrete. *Int J Civil, Environ Struct Constr Archit Eng* 2011; 5: 64–70.
28. Noushini A and Castel A. The effect of heat-curing on transport properties of low-calcium fly ash-based geopolymer concrete. *Constr Build Mater* 2016; 112: 464–477.
29. di Prisco M, Felicetti R, Iorio F, et al. On the identification of SFRC tensile constitutive behaviour. *Fract Mech Concr Struct* 2001; 1: 541–548.
30. Marar K, Eren Ö and Celik T. Relationship between impact energy and compression toughness energy of high-strength fiber-reinforced concrete. *Mater Lett* 2001; 47: 297–304.
31. Daniel L and Loukili A. Behavior of high strength fiber-reinforced concrete beams under cyclic loading. *Struct J* 2002; 99: 248–256.
32. Song PS and Hwang S. Mechanical properties of high-strength steel fiber-reinforced concrete. *Constr Build Mater* 2004; 18: 669–673.
33. Swamy RN and Stavrides H. Influence of fiber reinforcement on restrained shrinkage and cracking. *J Proc* 1979; 76: 443–460.

34. Grzybowski M and Shah SP. Shrinkage cracking of fiber reinforced concrete. *Mater J* 1990; 87: 138–148.
35. Gülşan ME, Alzeebaree R, Rasheed AA, et al. Development of fly ash/slag based self-compacting geopolymer concrete using nano-silica and steel fiber. *Constr Build Mater* 2019; 211: 271–283.
36. Sobolev K, Flores I, Hermosillo R, et al. Nanomaterials and nanotechnology for high-performance cement composites. In: *Proceedings of ACI session on nanotechnology of concrete: recent developments and future perspectives*. Farmington Hills, MI: American Concrete Institute, 2006, pp.91–118.
37. Qing Y, Zenan Z, Deyu K, et al. Influence of nano-SiO2 addition on properties of hardened cement paste as compared with silica fume. *Constr Build Mater* 2007; 21: 539–545.
38. Li H, Xiao H, Yuan J, et al. Microstructure of cement mortar with nano-particles. *Compos Part B Eng* 2004; 35: 185–189.
39. Çevik A, Alzeebaree R, Humur G, et al. Effect of nano-silica on the chemical durability and mechanical performance of fly ash based geopolymer concrete. *Ceram Int* 2018; 44: 12253–12264.
40. Senff L, Labrincha JA, Ferreira VM, et al. Effect of nano-silica on rheology and fresh properties of cement pastes and mortars. *Constr Build Mater* 2009; 23: 2487–2491.
41. Görhan G, Aslaner R and Şinik O. The effect of curing on the properties of metakaolin and fly ash-based geopolymer paste. *Compos Part B Eng* 2016; 97: 329–335.
42. Belkowitz JS (2009) An investigation of nano silica in the cement hydration process (Order No. 1470786). Available from ProQuest Dissertations & Theses Global. (304872705). Retrieved from https://www.proquest.com/dissertations-theses/investigation-nano-silica-cement-hydration/docview/304872705/se-2?accountid = 150320
43. Alzeebaree R, Gülsan ME, Nis A, et al. Performance of FRP confined and unconfined geopolymer concrete exposed to sulfate attacks. *Steel Compos Struct* 2018; 29: 201–218.
44. Silva F, Arezes P and Swuste P. Risk management: controlling occupational exposure to nanoparticles in construction. In: *Nanotechnology in eco-efficient construction*. Sawston: Woodhead Publishing, 2019, pp.755–784.
45. Olivia M and Nikraz H. Properties of fly ash geopolymer concrete designed by Taguchi method. *Mater Des* 2012; 36: 191–198.
46. Memon FA, Nuruddin MF, Khan S, et al. Effect of sodium hydroxide concentration on fresh properties and compressive strength of self-compacting geopolymer concrete. *J Eng Sci Technol* 2013; 8: 44–56.
47. Corinaldesi V and Moriconi G. Characterization of self-compacting concretes prepared with different fibers and mineral additions. *Cem Concr Compos* 2011; 33: 596–601.
48. EFNARC M (2005) The European Guidelines for Self Compacting Concrete Specification, Production, and Use. European Federation for Specialist Construction Chemicals and Concrete systems.
49. Niş A and Altındal İ. Compressive strength performance of alkali activated concretes under different curing conditions. *Period Polytech Civil Eng* 2021; 65: 556–565.
50. ASTM C39/C39M-01. *Standard test method for compressive strength of cylindrical concrete specimens*. West Conshohocken, PA: ASTM International, 2003.
51. EN B 12350-8. *Testing self compacting concrete: slump flow test*. London: British Standards Institution, 2010.
52. Ghanbari A and Karihaloo BL. Prediction of the plastic viscosity of self-compacting steel fibre reinforced concrete. *Cem Concr Res* 2009; 39: 1209–1216.
53. Belkowitz JS, Belkowitz WLB, Nawrocki K, et al. Impact of nanosilica size and surface area on concrete properties. *ACI Mater J* 2015; 112: 419–427.
54. Nili M and Afroughsabet V. Combined effect of silica fume and steel fibers on the impact resistance and mechanical properties of concrete. *Int J Impact Eng* 2010; 37: 879–886.
55. Nis A, Özyurt N and Özturan T. Variation of flexural performance parameters depending on specimen size and fiber properties. *J Mater Civ Eng* 2020; 32: 4020054.
56. Bayramov F, Taşdemir C and Taşdemir MA. Optimisation of steel fibre reinforced concretes by means of statistical response surface method. *Cem Concr Compos* 2004; 26: 665–675.
57. Mohammadi Y, Singh SP and Kaushik SK. Properties of steel fibrous concrete containing mixed fibres in fresh and hardened state. *Constr Build Mater* 2008; 22: 956–965.
58. Yazici S, Inan G and Tabak V. Effect of aspect ratio and volume fraction of steel fiber on the mechanical properties of SFRC. *Constr Build Mater* 2007; 21: 1250–1253.
59. Wang Y, Li VC and Backer S. Experimental determination of tensile behavior of fiber reinforced concrete. *Mater J* 1990; 87: 461–468.
60. Campione G, Cucchiara C, La Mendola L, et al. Steel–concrete bond in lightweight fiber reinforced concrete under monotonic and cyclic actions. *Eng Struct* 2005; 27: 881–890.
61. Chen B and Liu J. Properties of lightweight expanded polystyrene concrete reinforced with steel fiber. *Cem Concr Res* 2004; 34: 1259–1263.
62. Somna K and Bumrongjaroen W. Effect of external and internal calcium in fly ash on geopolymer formation. *Dev Strateg Mater Comput Des II Ceram Eng Sci Proc* 2011; 32: 1–16.
63. Abu-Lebdeh T, Hamoush S, Heard W, et al. Effect of matrix strength on pullout behavior of steel fiber reinforced very-high strength concrete composites. *Constr Build Mater* 2011; 25: 39–46.
64. Kayali O, Haque MN and Zhu B. Some characteristics of high strength fiber reinforced lightweight aggregate concrete. *Cem Concr Compos* 2003; 25: 207–213.
65. Nanni A. Splitting-tension test for fiber reinforced concrete. *ACI Mater J* 1988; 85: 229–233.
66. Alzeebaree R, Çevik A, Mohammedameen A, et al. Mechanical performance of FRP-confined geopolymer concrete under seawater attack. *Adv Struct Eng* 2020; 23: 1055–1073.
67. Gülsan ME, Mohammedameen A, Sahmaran M, et al. Effects of sulphuric acid on mechanical and durability properties of ECC confined by FRP fabrics. *Adv Concr Constr* 2018; 6: 199.